

TARGET-BASED AND FEATURE-BASED CALIBRATION OF LOW-COST DIGITAL CAMERAS WITH LARGE FIELD-OF-VIEW

Fangning He, Ph.D. student
Ayman Habib, Professor
Lyles School of Civil Engineering
Purdue University, 550 Stadium Mall Dr., West Lafayette, IN 47907, USA
he270@purdue.edu
ahabib@purdue.edu

Abstract

Nowadays, both target-based and feature-based camera calibration approaches have been developed and investigated for different photogrammetric tasks. However, almost no research has been conducted on comparing these approaches for low-cost large-field-of-view (LFOV) digital cameras. In this paper, a two-step procedure is utilized for the comparative analysis of the derived camera calibration parameters of a low-cost LFOV camera. First, both target-based and feature-based camera calibration procedures are carried out. Then, a stability analysis tool is applied to evaluate the similarity/difference between the derived camera calibration parameters in the first step. In order to test the proposed procedure, a GoPro Hero 3+ Black Edition Camera was utilized. Four real datasets with different image configurations were acquired for the camera calibration. The final stability analysis on the utilized GoPro camera indicates that we obtain similar estimates of the camera's interior orientation parameters (IOPs) from both target-based and feature-based camera calibration.

Keywords: Camera Calibration, Interior Orientation Parameters, Structure from Motion, Stability Analysis

INTRODUCTION

Recently, several low-cost LFOV digital cameras have been introduced to the market. For example, the GoPro camera, which is primarily designed for recording extreme activities, is one of the most popular low-cost LFOV cameras. Since these cameras are easy to handle and capable of providing high resolution images/videos even under extreme conditions, research efforts have been exerted towards their utilization for photogrammetric applications. However, due to the significant image distortions caused by the wide-angle lens, camera calibration has to be carried out prior to the data acquisition using these low-cost LFOV cameras for photogrammetric applications.

The objective of the camera calibration is to derive an accurate estimate of the internal characteristics of the utilized camera. The internal characteristics, which are commonly known as the IOPs, usually include the principal point offsets, principal distance, and additional distortion parameters (e.g., radial lens distortions, and de-centering lens distortions). In the past decades, camera calibration has been well developed in both the photogrammetric and computer vision communities (Fraser, 1997; Zhang, 2000). Nowadays, the most commonly employed technique for digital camera calibration is a bundle adjustment. As far as such calibration technique is concerned, one of two approaches can be adopted. In the first approach, signalized targets – on a calibration test field - are utilized. These targets are precisely established and surveyed. In order to facilitate the automation of the camera calibration, coded signalized targets have been proposed and implemented for automated matching of corresponding features and image orientation recovery. For example, Habib et al. (2013) investigated the automated detection and localization of different types of signalized targets (e.g., checkerboard and circular targets). Then, a semi-automated approach was proposed for identifying corresponding targets in different images. Although, target-based camera calibration provides reliable estimates for the camera IOPs, the preparation of a calibration test field remains inconvenient in some situations. For example, it is inconvenient to set-up a target field for cameras with long focal length. In the second approach, Structure-from-Motion (SfM) algorithms, which have been initiated by the computer vision community, is adopted. Since SfM automates the process of feature matching and image orientation recovery, the feature-based camera calibration can be implemented using the SfM without the requirement for signalized targets. Another advantage of the feature-based camera calibration is that more feature points can be involved into the bundle adjustment process to support the estimation of the camera IOPs. By using state-of-the-art feature matching techniques, the feature-based camera calibration can easily derive thousands of feature points from a texture-rich object. In contrast,

the target-based camera calibration usually employs 100 or so targets. Several research efforts have been conducted on feature-based camera calibration. Barazzetti et al. (in 2011) investigated the potential of feature-based camera calibration. In their research, a fully automated procedure was proposed for self-camera calibration and image orientation evaluation in the absence of targets. Stamatopoulos and Fraser (2014) demonstrated that calibration parameters derived from a feature-based approach using the SfM is of equal accuracy when compared to the conventional target-based approach. However, these studies did not provide quantitative estimates to describe the degree of similarity between target-based/feature-based IOPs under different operational conditions.

Although both target-based and feature-based camera calibration approaches have been adopted for various applications, it is important to note that almost no research has been conducted on comparing these approaches when dealing with a low-cost LFOV camera. Therefore, this research is dealing with a comparative analysis of the calibration parameters derived from different calibration approaches for a low-cost LFOV camera. More specifically, the research will be focusing on the following issues:

- The performance of target-based camera calibration for low-cost LFOV digital cameras,
- The performance of feature-based camera calibration for low-cost LFOV cameras, and
- Evaluating the similarities/differences between the derived camera calibration parameters from different approaches.

To address these issues, the utilized methodology is introduced in the next section. Afterwards, experimental results using real datasets are discussed. Finally, the drawn conclusions as well as recommendations for future work are presented.

METHODOLOGY

The objective of this research is comparative analysis of the derived camera calibration parameters from target-based and feature-based camera calibration approaches. In order to achieve this objective, a two-step procedure is proposed. First, both target-based and feature-based camera calibration are carried out for a low-cost LFOV camera. Then, a stability analysis tool is applied to evaluate the similarity/difference between the camera calibration parameters from these procedures.

Calibration Model

The USGS Simultaneous Multi-frame Analytical Calibration (SMAC) Distortion Model is utilized for the camera calibration in this research. For the SMAC model, all image points (x, y) must be referenced to the image coordinate system and then translated to the principal point (x_p, y_p) as in Equation 1.

$$\begin{aligned}\bar{x} &= x - x_p \\ \bar{y} &= y - y_p\end{aligned}\quad (1)$$

For the distortion parameters, radial lens distortion and de-centering lens distortion are considered. Radial lens distortion is caused by large off-axial angles and lens manufacturing flaws. It takes place along a radial direction from the principal point. Due to the utilization of a wide-angle lens, the radial lens distortion is more significant in LFOV cameras. According to the SMAC model, the correction for the radial lens distortion $(\Delta x_{RLD}, \Delta y_{RLD})$ can be expressed as in Equation 2 using the coefficients (K_0, K_1, K_2, K_3) .

$$\begin{aligned}\Delta x_{RLD} &= \bar{x}[K_0 + K_1(r^2 - R_0^2) + K_2(r^4 - R_0^4) + K_3(r^6 - R_0^6)] \\ \Delta y_{RLD} &= \bar{y}[K_0 + K_1(r^2 - R_0^2) + K_2(r^4 - R_0^4) + K_3(r^6 - R_0^6)]\end{aligned}\quad (2)$$

Where: $r = \sqrt{\bar{x}^2 + \bar{y}^2}$; K_0, K_1, K_2 and K_3 are the radial lens distortion parameters; R_0 is a camera-specific constant.

De-centering lens distortion is caused by misalignment of the elements of the lens system along the camera's optical axis. The de-centering lens distortion has radial and tangential components. To evaluate the de-centering lens distortion $(\Delta x_{DLD}, \Delta y_{DLD})$ for the measured points, one can use the coefficients (P_1, P_2, P_3) as shown in Equation 3.

$$\begin{aligned}\Delta x_{DLD} &= P_1(r^2 + 2\bar{x}^2) + 2P_2\bar{x}\bar{y} \\ \Delta y_{DLD} &= 2P_1\bar{x}\bar{y} + P_2(r^2 + 2\bar{y}^2)\end{aligned}\quad (3)$$

Where: P_1 and P_2 are the de-centering lens distortion parameters.

Target-based Camera Calibration

A test field with signalized targets is established for target-based camera calibration. In order to achieve reliable estimates of the camera's IOPs, convergent image configuration is employed. Then, the signalized targets are manually measured or automatically localized in different images. Since the initial approximation of the images' exterior orientation parameters (EOPs) is required for the bundle adjustment, the quaternion-based single photo resection algorithm, which is developed by Mazaheri and Habib (2015), is adopted in this research for initial recovery of the EOPs of the involved images. Finally, a bundle adjustment with self-calibration is carried out for the estimation of the utilized camera IOPs.

Feature-based Camera Calibration

The feature-based camera calibration is performed using the SfM approach developed by He and Habib (2014). This approach is based on a two-step linear solution for the initial recovery of the image EOPs. In the first step, point feature correspondences are identified, and then the relative orientation parameters (ROPs) relating stereo-images are computed from the derived conjugate points. In the second step, a local reference coordinate frame is established. Afterwards, the EOPs of the remaining images are sequentially recovered through an incremental augmentation process. A work flow of the proposed approach is illustrated in Figure 1.

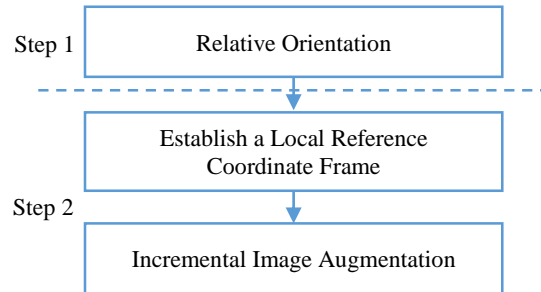


Figure 1. Workflow of the utilized SfM approach

The estimation of ROPs requires the identification of conjugate points in the set of available images. The Scale-Invariant Feature Transform (SIFT) detector/descriptor is used to identify corresponding point features within the stereo-images. Afterwards, using initial approximations for the camera's calibration parameters, the ROPs are derived first through a linear approach that establishes the essential matrix. Finally, the ROPs are refined through the coplanarity model (Mikhail et al., 2001).

Once the ROPs for all possible stereo-pairs are estimated, an incremental approach is utilized for the initial recovery of the image EOPs. The incremental approach is initiated by defining a local coordinate frame. In this research, the local reference frame is established using an image triplet that satisfies both good compatibility configuration and a large number of corresponding points.

Once the local coordinate frame is established, the images are sequentially augmented into a block. In this research, the utilized approach incorporates a linear approach for the estimation of the image EOPs (He and Habib, 2014). To be more specific, the rotational component of the EOPs for the augmented images are estimated using a quaternion-based linear approach. Then, the positional component of the EOPs for the augmented images is derived through an intersection of multiple vectors, which are the translation vectors connecting the referenced and unreferenced images. In order to reduce the effects of error propagation, at each step of the image incremental augmentation, only the image that exhibits the highest compatibility with the previous referenced imagery is selected and referenced into the local frame.

Interpretation of Camera Calibration

In this research, both the square root of a posteriori variance (σ_0) and variance of estimated IOPs are utilized to interpret target-based and feature-based camera calibration. A posteriori variance is a measure of the quality of fit between the observed quantities and the estimated quantities derived from the bundle adjustment. The square root of a posteriori variance (σ_0) is considered as the average magnitude of the image residuals. For an acceptable calibration, σ_0 must be within the range of the expected error in the image coordinate measurements (the noise in the data). The variances of the estimated IOPs from the bundle adjustment are a measure of the quality of these estimates. For an

adequate estimation of the derived IOPs from the camera calibration procedure, their standard deviations should be in the range of a few microns, which is a fraction of the pixel size of the camera.

Stability Analysis of the Estimated Interior Orientation Parameters

The main objective of this research is comparative performance analysis of different calibration approaches for a low-cost LFOV camera. Therefore, qualitative and quantitative evaluation methodologies need to be established for the comparative analysis of the derived camera calibration parameters from the target-based and feature-based camera calibration approaches. The qualitative evaluation can be conducted by evaluating the similarity of the numerical values of the derived camera IOPs. In this research, the quantitative evaluation of derived IOPs is performed using the camera stability analysis approach proposed by Habib et al. (2006). The basic idea of this stability analysis is based on the ultimate goal of the camera calibration procedure, which aims at minimizing the differences between the bundle of reconstructed light rays and the bundle of incident light rays onto the camera at the moment of exposure. Therefore, in this approach, the proposed IOP similarity analysis is based evaluating the degree of similarity between the reconstructed bundles of light rays from two different IOPs sets.

In this research, the derived IOPs from target-based and feature-based camera calibration are compared. The comparison starts by reconstructing two bundles from these two IOPs sets. In order to do so, a regular grid is initially defined along a virtual image plane. Then, distortion-free grid vertices are generated by using the two IOPs sets. Afterwards, two bundles of light rays are reconstructed by connecting the perspective center, which is defined by the principal distance and the principal point coordinates, to the distortion-free coordinates of the grid vertices. Finally, the degree of similarity between the two bundles is evaluated. The Square Root of the Variance Component ($RMSE_{offset}$) is the measure used to assess the similarity between the two bundles. It is defined as the average spatial offset between corresponding light rays within the two reconstructed bundles along the image plane after the alignment of the two bundles. The two IOPs sets will be deemed similar if the $RMSE_{offset}$ is within the noise range of the image coordinate measurements, which is usually in the range of one pixels.

EXPERIMENTAL RESULTS

In order to perform the comparative analysis of the derived camera calibration parameters for a low-cost LFOV camera, we conducted several camera calibration experiments using real image datasets that have been captured in different configurations.

Dataset Description

The utilized datasets in this research are acquired by a GoPro Hero 3+ Black Edition camera (See Figure 2). There are several imaging modes for the utilized GoPro Camera. In this research, only the medium field-of-view mode is utilized. The specifications of the GoPro Camera are shown in Table 1.

Table 1. The specifications of the GoPro Hero 3+ Black Edition Camera

	Image Mode	Image Size	Vertical FOV (°)	Horizontal FOV (°)	Pixel Size (mm)	Nominal Focal Length (mm)
GoPro Hero 3+ Black Edition	Medium FOV	3000 x 2250	72.2	94.4	0.00155	3



Figure 2. GoPro Hero 3+ Black Edition Camera

For the target-based camera calibration, two sets of images are acquired. For each image dataset, a total of 18 images of a 2D calibration test field with 35 targets are captured with the same image network configuration. A schematic illustration of the test field and the location and orientation of the acquired images are shown in Figure 3. Figure 4(a) illustrates one of the captured images of the test field.

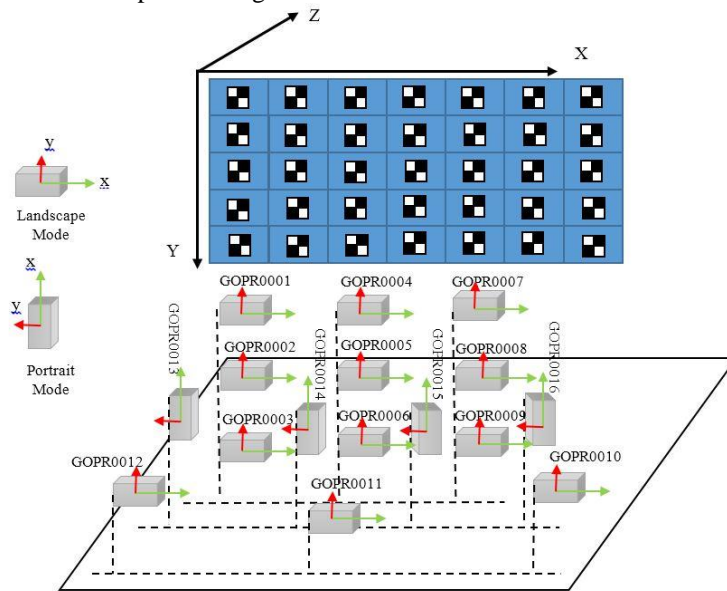


Figure 3. The calibration test field together with the position and orientation of the captured images for the target-based camera calibration

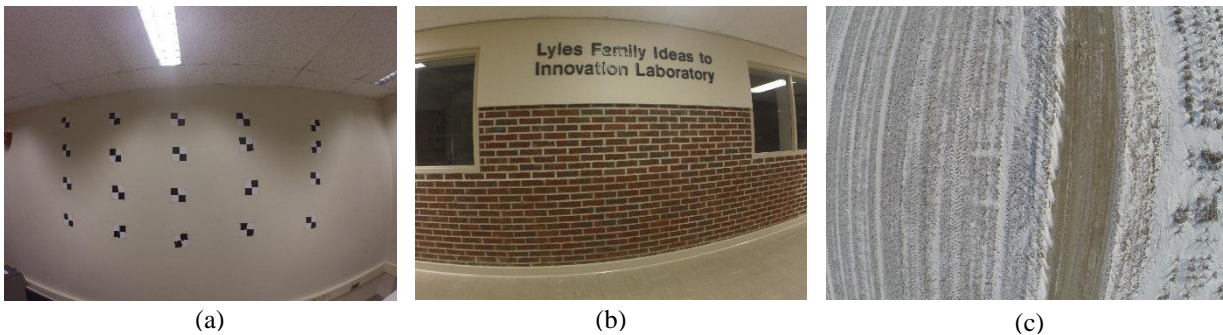


Figure 4 (a) A sample image for the calibration test field, (b) a sample image for the indoor image dataset, and (c) a sample image for the UAV image dataset

For the feature-based camera calibration, two image datasets (See Figures 4(b) and 4(c)) were acquired by the GoPro camera under different operational conditions. The first image dataset includes a total number of 25 images of an indoor environment. The second image dataset includes a total number of 38 images acquired by the same GoPro camera mounted on a DJI Phantom2 UAV. By using the proposed SfM approach, 14,047 points are reconstructed from the indoor image dataset, and 157,321 points are reconstructed from the UAV image dataset. The derived position and orientation of the captured images as well as the reconstructed point clouds from both image datasets are shown in Figure 5.

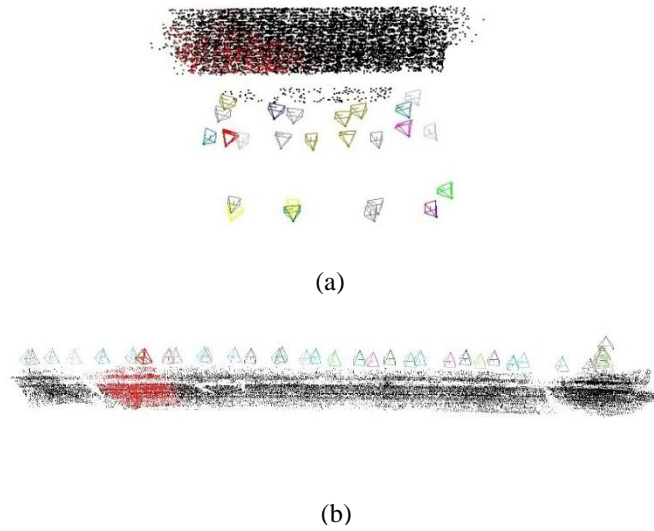


Figure 5. Reconstructed points and position and orientation of the involved images for (a) indoor image dataset, and (b) UAV image dataset.

Derived Camera Calibration Parameters

As it has been mentioned earlier, the SMAC model supports the parameter of R_0 , which is a camera-specific constant. In this research, the SMAC model with R_0 values of 0 and 3 mm are utilized for both the target-based and feature-based camera calibration approaches. Only K_1 , K_2 and K_3 are considered as the distortion parameters. Table 2 illustrates the derived square root of a posteriori variance (σ_0) of all four image datasets using different camera calibration approaches with different R_0 values. One can note that the derived σ_0 values are all smaller than one pixel size (0.00155 mm), which indicates that no blunders are present and the utilized SMAC model is appropriate. The derived IOPs from both the target-based and feature-based calibration approaches as well as the standard deviation of the derived IOPs are reported in Tables 3, 4, 5, and 6. One can note that the standard deviations of the estimated IOPs are all in the range of a few microns. These results indicate that the derived IOPs are acceptable.

Table 2. The derived square root of a posteriori variance σ_0 for different calibration experiments

Approaches	Image Dataset	σ_0 ($R_0 = 0$ mm)	σ_0 ($R_0 = 3$ mm)
Target-based Calibration	Target Dataset 1	1.0560e-003mm	9.1037e-004 mm
	Target Dataset 2	6.6780e-004 mm	8.6581e-004 mm
Feature-based Calibration	Indoor Dataset	1.3315e-003mm	7.6845e-004 mm
	UAV Dataset	9.9049e-004mm	9.2861e-004 mm

Table 3. Estimated IOPs and their standard deviations from the first target-based image dataset

R0 = 0 mm				R0 = 3 mm			
x_p (mm)	-7.3634e-02	σ_{x_p} (mm)	± 0.0014	x_p (mm)	-7.2726e-02	σ_{x_p} (mm)	± 0.0012
y_p (mm)	8.7821e-02	σ_{y_p} (mm)	± 0.0014	y_p (mm)	9.4307e-02	σ_{y_p} (mm)	± 0.0012
c (mm)	2.6989	σ_c (mm)	± 0.0022	c (mm)	1.7427	σ_c (mm)	± 0.0030
K_1 (mm ⁻²)	-3.9445e-02	σ_{K_1} (mm ⁻²)	$\pm 3.0882e-04$	K_1 (mm ⁻²)	-2.5630e-02	σ_{K_1} (mm ⁻²)	$\pm 2.3183e-004$
K_2 (mm ⁻⁴)	-1.1881e-03	σ_{K_2} (mm ⁻⁴)	$\pm 9.5094e-05$	K_2 (mm ⁻⁴)	-7.1433e-04	σ_{K_2} (mm ⁻⁴)	$\pm 8.2658e-05$
K_3 (mm ⁻⁶)	-1.3126e-04	σ_{K_3} (mm ⁻⁶)	$\pm 9.3738e-06$	K_3 (mm ⁻⁶)	-9.0405e-05	σ_{K_3} (mm ⁻⁶)	$\pm 7.9050e-06$

Table 4. Estimated IOPs and their standard deviations from the second target-based image dataset

R0 = 0 mm				R0 = 3 mm			
x_p (mm)	-7.7553e-02	σx_p (mm)	± 0.0016	x_p (mm)	-7.0273e-02	σx_p (mm)	± 0.0012
y_p (mm)	8.4873e-02	σy_p (mm)	± 0.0016	y_p (mm)	9.1216e-002	σy_p (mm)	± 0.0012
c (mm)	2.6987	σc (mm)	± 0.0024	c (mm)	1.7426	σc (mm)	± 0.0030
K_1 (mm ⁻²)	-3.9280e-02	σK_1 (mm ⁻²)	$\pm 4.6582e-04$	K_1 (mm ⁻²)	-2.5579e-02	σK_1 (mm ⁻²)	$\pm 1,1891e-004$
K_2 (mm ⁻⁴)	-1.2408e-03	σK_2 (mm ⁻⁴)	$\pm 4.6643e-05$	K_2 (mm ⁻⁴)	-7.2438e-04	σK_2 (mm ⁻⁴)	$\pm 4.0953e-05$
K_3 (mm ⁻⁶)	-1.2604e-04	σK_3 (mm ⁻⁶)	$\pm 9.7573e-06$	K_3 (mm ⁻⁶)	-8.9327e-05	σK_3 (mm ⁻⁶)	$\pm 3.9249e-06$

Table 5. Estimated IOPs and their standard deviation from the indoor image dataset

R0 = 0 mm				R0 = 3 mm			
x_p (mm)	-8.3140e-02	σx_p (mm)	± 0.0001	x_p (mm)	3.0273e-02	σx_p (mm)	± 0.0003
y_p (mm)	1.0705e-01	σy_p (mm)	± 0.0001	y_p (mm)	8.3383e-02	σy_p (mm)	± 0.0003
c (mm)	2.6991	σc (mm)	± 0.0001	c (mm)	1.7406	σc (mm)	± 0.0006
K_1 (mm ⁻²)	-3.9082e-02	σK_1 (mm ⁻²)	$\pm 1.8518e-005$	K_1 (mm ⁻²)	-2.5716e-02	σK_1 (mm ⁻²)	$\pm 2.3417e-05$
K_2 (mm ⁻⁴)	-1.2736e-03	σK_2 (mm ⁻⁴)	$\pm 4.9930e-006$	K_2 (mm ⁻⁴)	-5.6784e-04	σK_2 (mm ⁻⁴)	$\pm 3.7672e-06$
K_3 (mm ⁻⁶)	-1.2232e-04	σK_3 (mm ⁻⁶)	$\pm 8.7478e-007$	K_3 (mm ⁻⁶)	-1.0037e-04	σK_3 (mm ⁻⁶)	$\pm 4.0842e-07$

Table 6. Estimated IOPs and their standard deviations from the UAV image dataset

R0 = 0 mm				R0 = 3 mm			
x_p (mm)	-8.1679e-02	σx_p (mm)	± 0.0010	x_p (mm)	-2,9104e-02	σx_p (mm)	± 0.0009
y_p (mm)	8.7128e-02	σy_p (mm)	± 0.0010	y_p (mm)	1.12092e-01	σy_p (mm)	± 0.0008
c (mm)	2.6992	σc (mm)	± 0.0019	c (mm)	1.7412	σc (mm)	± 0.0031
K_1 (mm ⁻²)	-3.9721e-02	σK_1 (mm ⁻²)	$\pm 3.1175e-04$	K_1 (mm ⁻²)	-2.5528e-02	σK_1 (mm ⁻²)	$\pm 2.3466e-04$
K_2 (mm ⁻⁴)	-1.0895e-03	σK_2 (mm ⁻⁴)	$\pm 9.9240e-05$	K_2 (mm ⁻⁴)	-7.9134e-04	σK_2 (mm ⁻⁴)	$\pm 8.7787e-05$
K_3 (mm ⁻⁶)	-1.4145e-04	σK_3 (mm ⁻⁶)	$\pm 1.0060e-05$	K_3 (mm ⁻⁶)	-8.2917e-05	σK_3 (mm ⁻⁶)	$\pm 8.6356e-06$

Stability Analysis of the Derived IOPs

The objective of the last stage of the experimental results is to test and evaluate the similarity of the derived IOP sets. The similarity test is performed using the stability analysis, which has been introduced in previous sections. In this research, two different comparisons are carried out. For the first comparison, the IOP sets, which are derived from the same camera calibration approach – i.e., either target-based or feature-based, are compared. For the second comparison, we investigate the similarity between the estimated IOP sets, which are derived from different camera calibration approaches. The values of derived $RMSE_{offset}$ from the stability analysis are reported in Table 6. From the reported numbers in Table 6, one can conclude the following:

- The derived IOPs from the same camera calibration approach (i.e., target-based or feature-based) exhibit a similarity at the one pixel level (0.00155 mm). This implies that the utilized GoPro camera has stable IOPs.
- The $RMSE_{offset}$ values when comparing the IOPs from the target-based and feature-based calibration are all less than a pixel (0.00155 mm). This indicates that the IOPs derived from different camera calibration

approaches are considered to be similar. Therefore, we can conclude that there is a high level of similarity between the derived IOPs from target-based and feature-based camera calibration.

Table 7. The $RMSE_{offset}$ between the derived IOPs

	IOP_1	IOP_2	$RMSE_{offset}$ ($R0 = 0$ mm)	$RMSE_{offset}$ ($R0 = 3$ mm)
Comparison 1	Target Dataset 1	Target Dataset 2	0.00068 mm	0.00182 mm
	Indoor Dataset	UAV Dataset	0.00146 mm	0.00134 mm
Comparison 2	Target Dataset 1	Indoor Dataset	0.00143 mm	0.00105 mm
	Target Dataset 1	UAV Dataset	0.00114 mm	0.00113 mm
	Target Dataset 2	Indoor Dataset	0.00086 mm	0.00141 mm
	Target Dataset 2	UAV Dataset	0.00092 mm	0.00202 mm

CONCLUSIONS AND RECOMMENDATIONS

In this paper, we utilized two different approaches – target-based and feature-based camera calibration – for the calibration of a low-cost LFOV camera. Then, a comparative analysis was performed on the derived IOPs. For the experimental tests, a GoPro Hero 3+ Black Edition camera was utilized. In order to evaluate the similarity between the derived IOPs, four real datasets are tested. These datasets were acquired with different image configurations. By performing a stability analysis on the derived IOPs, we can draw the conclusion that there is a good level of similarity between the derived IOPs from both target-based and feature-based camera calibration.

It is important to note that we only tested the medium field-of-view mode of the GoPro Camera in this research. For future work, more experiments will be carried out on the super-wide mode of the GoPro Camera.

REFERENCES

- Barazzetti, L., Remondino, F., Scaioni, M., 2011. Automated and accurate orientation of complex image sequences. *Int Arch. Photogramm. Remote Sens. Spat. Inf. Sci.* 38.
- Fraser, C.S., 1997. Digital camera self-calibration. *ISPRS J. Photogramm. Remote Sens.* 52, 149–159.
- Habib, A., Lari, Z., Kwak, E., Al-Durgham, K., 2013. AUTOMATED DETECTION, LOCALIZATION, AND IDENTIFICATION OF SIGNALIZED TARGETS AND THEIR IMPACT ON DIGITAL CAMERA CALIBRATION. *Rev. Bras. Cartogr.*
- Habib, A., Pullivelli, A., Mitishita, E., Ghanma, M., Kim, E.-M., 2006. Stability analysis of low-cost digital cameras for aerial mapping using different georeferencing techniques. *Photogramm. Rec.* 21, 29–43.
- He, F., Habib, A., 2014. Linear Approach for Initial Recovery of the Exterior Orientation Parameters of Randomly Captured Images by Low-Cost Mobile Mapping Systems. *ISPRS-Int. Arch. Photogramm. Remote Sens. Spat. Inf. Sci.* 1, 149–154.
- Mazaheri, M., Habib, A., 2015. Quaternion-based Solutions for the Single Photo Resection Problem. *Photogramm. Eng. Remote Sens.* 81, 209–217.
- Mikhail, E.M., Bethel, J.S., McGlone, J.C., 2001. *Introduction to modern photogrammetry*. John Wiley & Sons Inc.
- Stamatopoulos, C., Fraser, C.S., 2014. AUTOMATED TARGET-FREE NETWORK ORIENTATION AND CAMERA CALIBRATION. *ISPRS Ann. Photogramm. Remote Sens. Spat. Inf. Sci.* 1, 339–346.
- Zhang, Z., 2000. A flexible new technique for camera calibration. *Pattern Anal. Mach. Intell. IEEE Trans. On* 22, 1330–1334.